Raman Identification of Multiple Melting Peaks of Polyethylene

Ying Jin,[†] *Anthony P. Kotula,*[‡] *Chad R. Snyder,*[‡] *Angela R. Hight Walker,*[§] *Kalman B. Migler,*[‡] *and Young Jong Lee**[,†]

[†]Biosystems & Biomaterials Division, [‡]Materials Science & Engineering Division, and [§]Engineering Physics Division, National Institute of Standards and Technology, Gaithersburg, Maryland 20899

ABSTRACT

Multiple melting peaks of high-density polyethylene produced by complex thermal pre-treatment are investigated with variable temperature Raman spectroscopy and differential scanning calorimetry (DSC). We examine the origin of the observed multiple melting peaks with three possible model mechanisms: melting-recrystallization, pre-melting via mesophases, and melting of multi-thickness lamellae. We quantitatively analyze Raman spectral change associated with each melting peak with respect to temperature. The Raman spectral change is represented by a least squares moving-window (LSMW) method, which is effective in suppression of high-frequency derivative noise. The conformational similarity among multiple melting peaks strongly suggests that dominant melting occurs from the crystalline phase directly to the amorphous phase at all transitions. The observed multiple melting transitions are consistent with one-step melting of multi-thickness lamellae as the dominant origin. However, a two-dimensional Raman correlation

spectroscopy suggests that non-crystalline *trans*-rich conformations appear during the melting process, whose mass fraction is estimated as 10% or less. The combined techniques are shown to provide better insights into the melting process.

INTRODUCTION

Semicrystalline polymers, including polyethylene (PE) and polypropylene, are the largest group of commercial plastics. By melting and crystallization, the starting form of pellets or powder is manufactured into final products with an intended shape and properties. Better understanding of structural changes during the phase transitions becomes important not only for more effective production control but also for designing and inventing new products with unprecedented properties. However, there are challenges to understand the complex nature of the phase transitions of semi-crystalline polymers.[1] The solid phase exists in a mixture form of crystalline and amorphous phases, whose composition or crystallinity can vary depending on the molar mass distribution and its prior thermal and rheological history.[2, 3] The observed melting point is affected by not only the crystallinity and the higher order structures (orientation and lamellar thickness) but also the dynamics of heating and cooling.[4-6] In addition, the application of shear flow during crystallization , which is a critical part of commercial polymer processing techniques, is known to affect the melting point and dynamics of the melting transition.[7] Even slow shear ($< 3\ s^{-1}$) of PE of intermediate molecular weights (58,600 g/mol) will lead to variation in the crystallization kinetics and crystal orientation.[8] Higher shear rates can generate a shish-kebab structure, which has been noted in X-ray and transmission electron microscopy measurements.[9] For this reason, the study of melting transitions provides a unique

opportunity to investigate the solid phase before melting. Heterogeneity in the structural hierarchy and the dynamics of semi-crystalline polymers is thought to be related with often observed broad or multiple melting peaks.

Some X-ray studies suggest that heterogeneous melting of semi-crystalline polymer is due to the difference in molecular environment between the surface (or domain interface) and the bulk,[10, 11] while other X-ray and thermodynamic studies suggest that metastable phases between the crystalline and amorphous phases can result in multiple melting transitions.[12-15] In addition, reorganization and crystallization of mobile polymer chain segments can shift apparent melting peaks,[16-19] obscuring its interpretation. Crist has discussed extensively the challenges with using small angle X-ray scattering (SAXS) to model polymer crystal melting and has even argued that scattering can likely not provide information related to all of the changes occurring during melting.[20] The structural and dynamic complexity of semi-crystalline polymers makes it extremely challenging to study the underlying melting mechanisms only by univariate information from scattering and thermometric measurements.

PE is one of the model polymers widely studied for fundamental understanding of structure changes in the polymer melting, crystallization, and phase transition in general. PE melting has been investigated by many analytical methods, such as X-ray scattering,[11, 21-23] differential scanning calorimetry (DSC),[5, 24-27] near-IR,[28, 29] Raman,[21, 30, 31] dilatometry,[32] and nuclear magnetic resonance (NMR) spectroscopy.[33] However, some methods are based on univariate information, which is limited in identifying multiple phases simultaneously; other multivariate methods are not sufficiently sensitive to detect subtle changes associated

with heterogeneous melting transitions. For example, Raman spectroscopy has been widely used to characterize phase changes of polymers by simultaneously measuring multiple Raman bands associated with specific phases.[31, 34, 35] In particular, many Raman bands of PE and alkanes have been extensively studied for each phase.[31, 35, 36] Briefly, the amorphous phase exhibits relatively broad Raman bands due to disordered chain interactions and *gauche*-rich conformation. On the other hand, the crystalline phase is characterized with relatively narrow Raman bandwidth due to strict interchain interaction in the orthorhombic structure packing and *trans*-rich conformation. Some narrow Raman bands in alkanes remain after the orthorhombic crystalline bands disappear until the amorphous bands appear. These bands, called the non-crystalline consecutive *trans* (NCCT) bands,[35] represent rich *trans* conformers that are not in an orthorhombic crystalline packing. This type of identification of phase and conformation by Raman spectroscopy is straightforward when phase transitions are sufficiently separated and the phase-specific Raman characteristics are sufficiently different. However, a simple analysis of Raman intensities is typically not sufficiently sensitive to observe the subtle spectral changes in semi-crystalline polymers, whose observed melting transition is often broad and unresolvable.

Recently, Lee proposed a new spectral analysis method, called least squares moving-window (LSMW), as a versatile numerical differentiation tool that efficiently suppresses high-frequency differentiation noise.[37, 38] We use the LSMW method to analyze a series of variable temperature Raman spectra acquired from high-density polyethylene (HDPE). The improved signal-to-noise ratio of the derivative of Raman intensity with respect to temperature allows us to resolve the broad melting peak into multiple underlying peaks. Quantitative analysis of the Raman changes corresponding to the underlying melting peaks,

accompanied by thermal analysis, unravels the dominant mechanism for the broad and multi-peak melting transition of HDPE.

EXPERIMENTAL SECTION

Sample Preparation. The HDPE used in this study is NIST SRM 1475, which is a linear PE with a mass-average molar mass M_w = 53,000 g/mol and number-average molar mass M_n = 18,300 g/mol.[39] Pellets were first melt-pressed at (155 ± 1) °C into disks of thickness (1.0 ± 0.1) mm to make two samples.

Raman Spectroscopy. Two different Raman spectrometers were used to measure temperature dependent Raman spectra. Sample I was placed between the glass base and the stainless steel upper plate in a rheo-Raman microscope (Thermo Fisher Scientific, temperature uncertainty ± 0.1 °C).[40] Sample I was heated to 155 °C, compressed to the final thickness of (700 ± 30) μm, and cooled to room temperature by exposing the sample to ambient conditions. No flow was applied to Sample I. Sample I was (a) heated from 28.7 °C to 60 °C at 10 °C/min, (b) held at 60 °C for 10 min, (c) heated to 120 °C at 10 °C/min, (d) held at 120 °C for 10 min, and (e) finally heated to 140 °C at 0.1 °C/min. Raman spectra of Sample I were measured with the spectrometer of a DXR Raman microscope (Thermo Fisher Scientific; spectral resolution = 4 cm^{-1}), which was attached to the rheo-Raman microscope. The power of the excitation laser light of 532 nm at the sample was 10 mW. The Raman spectra of Sample I were measured with an increment of 0.1 °C between 120 °C and 140 °C at the scanning rate of 0.1 °C/min. Sample II was placed between the quartz disks of a shear cell (Linkam Scientific Instruments, CSS 450, temperature uncertainty within ± 0.1 °C), heated to 155 °C, and compressed to (700 ± 10) μm. Sample II was

crystallized by cooling at a rate of 30 °C/min from 155 °C to 128 °C, shearing the sample at temperature for 10 min at a rate of 1 s^{-1}, and then allowing the sample to crystallize for 120 min at 128 °C. The sample was cooled at 30 °C/min to 120 °C and immediately heated to 130 °C at 30 °C/min. The sample was then melted by heating the sample at a rate of 0.25 °C/min from 130 °C to 140 °C. Raman spectra of Sample II were measured with a triple grating Raman spectrometer (Horiba, T64000; spectral resolution = 0.8 cm^{-1}) in the 180° backscattering geometry. Lineally polarized light from a HeNe laser (632.8 nm) was focused into a spot with a diameter of 60 μm, and an average power of 15 mW. Raman spectra were measured with an increment of 0.25 °C between 130 °C and 140 °C. Each spectrum was detrended by a splined baseline calculated at four frequencies (952 cm^{-1}, 1240 cm^{-1}, 1340 cm^{-1}, and 1550 cm^{-1}). To compensate irregular scattering, the spectral intensity was scaled by the area of the CH_2 twisting band (1240 cm^{-1} to 1340 cm^{-1}).[31, 35]

Differential Scanning Calorimetry (DSC). DSC measurements ware performed on a TA Q1000 calorimeter equipped with a mechanical intercooler under a nitrogen atmosphere purge. Unless specifically mentioned, the heating rate was 0.1 °C/min to match that of variable temperature Raman measurements. Calibrations were performed according to the manufacturer's specifications.

Data Analysis. Principal component analysis (PCA) was performed with a commercial multivariate analysis package (Solo+MIA, Eigenvector Research, Inc). The Raman spectra were mean-centered before PCA. The first order derivative of spectral intensity with respect to temperature was calculated based on the LSMW by using the SLOPE function provided in the Microsoft Excel package. Two-dimensional correlation spectroscopy

(2DCOS) analysis was performed with 2D Shige, developed by Shigeaki Morita (Kwansei Gakuin University).

RESULTS AND DISCUSSION

Figure 1a displays selected Raman spectra acquired from Sample I (ambient cool from the melt with no shear) during heating, showing qualitative difference in peak positions and shape before and after melting. Most of the Raman peaks can be associated with the orthorhombic, consecutive *trans*, and amorphous conformations.[35, 41] Figure 1b shows plots of the area of the Lorentzian-fitted Raman peaks as a function of temperature. The 1419 cm^{-1} peak (the CH_2 bending mode), which represents the orthorhombic crystalline phase, decreases gradually as temperature increases. The narrow peak at 1295 cm^{-1} (the CH_2 twisting mode) is converted into the broad peak at 1302 cm^{-1} as the consecutive *trans* conformation is transformed into the amorphous phase. Similarly, the two narrow peaks at 1062 cm^{-1} and 1127 cm^{-1} (the C–C stretching mode) are transformed into the broad peak at 1080 cm^{-1} as the consecutive *trans* conformation becomes the amorphous phase. In Figure 1b, it is noted that the orthorhombic peak at 1419 cm^{-1} decreases at a similar rate with the consecutive *trans* peaks (1295 cm^{-1}, 1062 cm^{-1}, and 1127 cm^{-1}), which is quite different from the temperature dependence of the corresponding peaks in some *n*-alkane (n-$C_{21}H_{44}$).[41] For *n*-alkanes (n-C_nH_{2n+2}) of $9 \leq n \leq 39$, the orthorhombic peak at 1419 cm^{-1} decreases sharply at a temperature below the melting point, while the consecutive *trans* peaks decrease at the melting point.[36] Differences between HDPE and *n*-alkanes (n-C_nH_{2n+2}, $9 \leq n \leq 39$) are that the melting occurs over a wide temperature range; and that the

orthorhombic peak and the consecutive *trans* peaks decrease at a similar rate with temperature.

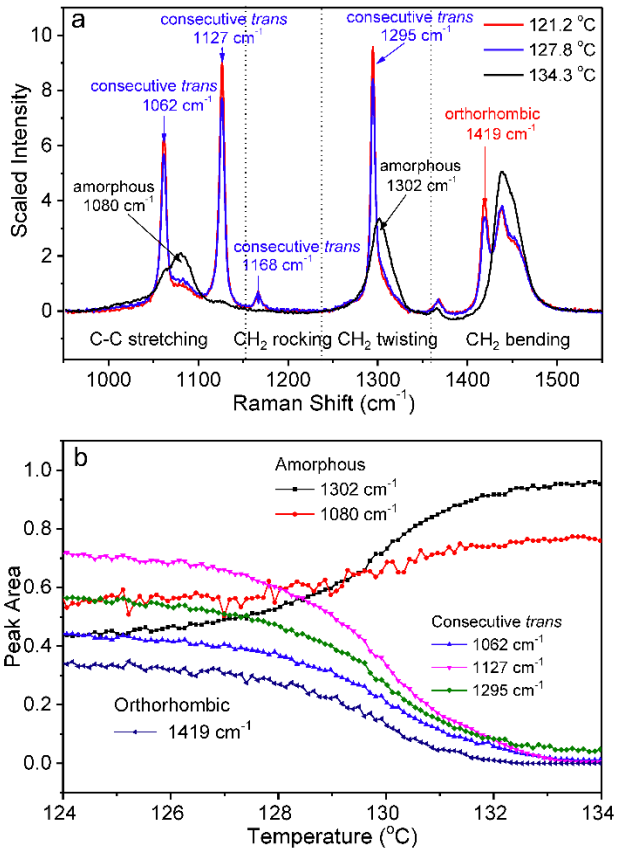

Figure 1. (a) Variable temperature Raman spectra of high-density polyethylene (HDPE) during melting. (b) The peak areas of selected Raman bands, which correspond to three molecular conformations: orthorhombic crystalline, consecutive *trans*, and amorphous.

To identify spectral changes associated with the broad phase transition, we performed a multivariate analysis for the whole series of Raman spectra. Principal component analysis (PCA) is widely used to find orthogonal spectral components (i.e., loadings) and their relative amplitudes (i.e. scores) with the orders of principal components determined from

the highest variance. The PCA score plots in Fig. 2a shows a gradual change with temperature, which is similar to the individual peak intensity changes. The large variance (>99%) of the first principal component indicates that the spectral change occurs between two states. This PCA result only reconfirms that the slow spectral change occurs from the crystalline and the consecutive *trans* conformation to the amorphous conformation but does not provide additional spectral information on multiple melting peaks.

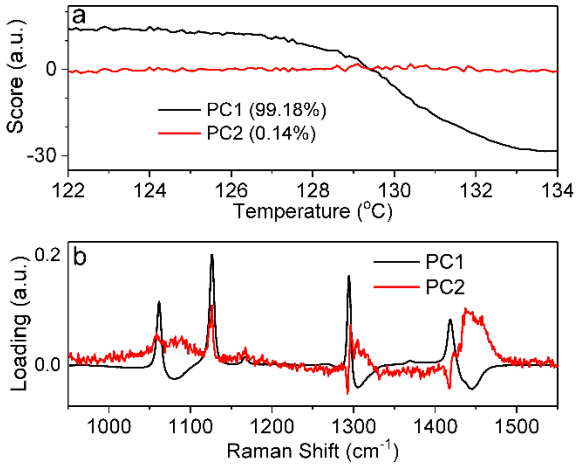

Figure 2. Principal component analysis (PCA) of the variable temperature Raman spectra of HDPE. (a) Scores and (b) loadings of the first two principal components (PC1 and PC2).

Figure 3a shows a DSC plot of Sample I, acquired at the same heating rate as the Raman measurement (0.1 °C/min). The DSC plot shows melting transition over a broad temperature range, which is like the Raman results shown in Figs. 1 and 2. Furthermore, the high signal-to-noise ratio of the DSC measurement can resolve the broad DSC curve into multiple peaks. These types of multiple broad melting peaks have been reported in

previous DSC studies of PE.[25, 33] Although the overall melting mechanisms of PE have been discussed with various types of mechanisms at the molecular level,[20, 25, 33] the origin(s) of the individual underlying peaks cannot be fully understood only by DSC and similar thermoanalytical methods due to insufficient structural information. Based on previous studies on PE melting, we propose three possible model mechanisms to explain the multiple melting peaks observed by DSC in Fig. 3a. Although the DSC plot of Fig. 3a can be fitted with either two or three peaks, for simplicity of discussion, we consider it as two melting peaks to illustrate the three model mechanisms in Fig. 4. First, in the melting-recrystallization model, lamellae thickening occurs via melt-crystallization[30, 42] at the lower temperature. Then, the thickened lamellae melt completely at the higher temperature. Before and after melting-recrystallization, the degree of crystallinity may change, but the lamellae are considered to be conformationally indistinguishable. The second model, called pre-melting via mesophases, assumes existence of a mesophase between the crystalline phase and the amorphous phase. At the lower temperature, the orthorhombic phase becomes the mesophase, which melts into the amorphous phase at the higher temperature. The mesophase is considered to be structurally or conformationally different from both the orthorhombic and amorphous phases. In the third model, the original orthorhombic phase contains a multimodal distribution of lamellae thicknesses. Thinner lamellae melt at a lower temperature, and thicker lamellae melt at a higher temperature. In this melting of multi-thickness lamellae model, all melting are considered as a single, conformationally identical transitions. The presence of such a distribution of lamellae could occur through a number of mechanisms including, for example, a secondary crystallization process where small crystallites form after (or during) the formation of the primary lamellar crystallites,

through the uncontrolled cooling process where rapid cooling results in a broad distribution of crystal size, or by a process similar to self-nucleation and successive annealing (SSA)[43] that occurred on heating to and holding at 120 °C prior to the DSC and Raman measurements. Because the larger area peak occurs at lower temperatures, secondary crystallization would be unlikely to have been the cause because it would correspond to a smaller total crystal fraction and would occur at lower temperatures. A very small endotherm was measured in the DSC starting at approximately 100 °C and continuing up to 120 °C, supporting the possibility of an SSA-type process (see Fig. S1). It should be noted that the actual melting process may involve two or more sub mechanisms occurring concurrently; however, our primary aim is to find the dominant origin of the multiple and broad melting peaks observed in DSC and Raman measurements.

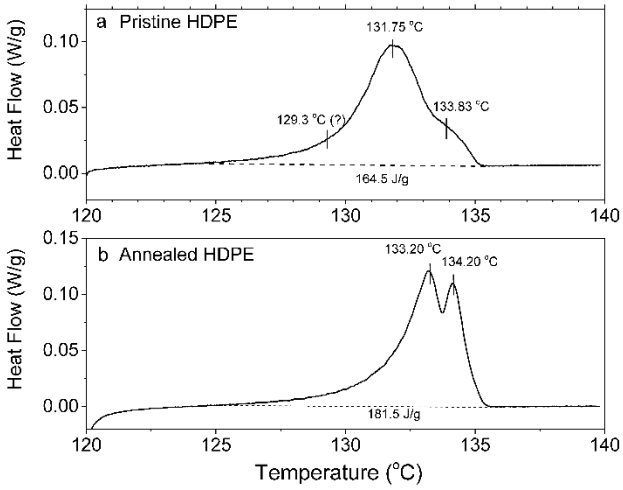

Figure 3. (a) A differential scanning calorimetry (DSC) heating trace of a pristine HDPE (sample I). (b) A DSC trace of an annealed HDPE, which was prepared from an additional sample with the identical thermal history as Sample I by first heating from room temperature to 60 °C at 10 °C/min, holding for 10 min, heating to 120 °C at 10 °C/min,

holding for 10 min, heating to 133 °C at 0.1 °C/min, and immediately cooling back to 120 °C at 1 °C/min. After the annealed sample was kept at 120 °C for 30 seconds, it was reheated for DSC measurement. For both (a) and (b), the DSC traces were measured at 0.1 °C/min.

In order to verify the model hypotheses, we performed DSC measurement of a different HDPE sample that was prepared with additional heat treatment of the same polymer as Sample I. Before the DSC measurement, the sample was heated to 133 °C, where the first melting was completed, and cooled back to 120 °C. In Fig. 3b, the DSC plot acquired during the second heating shows two distinct melting peaks, which are located at higher temperatures than those in Fig. 3a. In addition, the calculated degree of crystallinity increases from 56.1% for Sample I to 61.9% after the additional heat treatment. Because the increased melting temperature and crystallinity are among typical annealing effects,[24] the additional heat treatment can be considered as annealing. Separate Raman measurements were not performed due to the sensitivity of our samples to temperature and thermal history within the various instruments used for measurement.

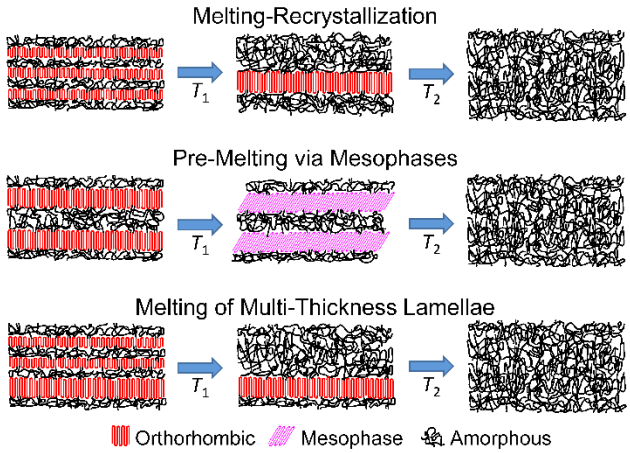

Figure 4. Three models used for discussion on the origin for observed multiple melting peaks of PE. In the melting-recrystallization model, orthorhombic lamellae thickening occurs at T_1 via melt-crystallization, and the thickened lamellae melt at T_2. In the pre-melting-via-mesophase model, the crystalline phase transforms into a mesophase at T_1 and melts into the amorphous phase at T_2. In the multi-thickness lamellae model, multiple melting temperatures correspond to with a multimodal thickness distribution of the orthorhombic lamellae in the crystalline phase.

First, the melting-recrystallization model is tested as a possible explanation of the second DSC result of the annealed HDPE. Like the DSC result of the pristine (non-annealed) HDPE sample, the initial heating above the lower melting temperature (T_1) would thicken lamellae from L to L' ($\geq L$) via melting-recrystallization. During the cooling, the thickened lamellae are expected to remain at the same thickness or become even thicker due to possible annealing during cooling from 133 °C to 120 °C for 13 min. If the melting-recrystallization model is correct, the annealing-thickened lamellae with thickness of L'' ($\geq L'$) should melt to the amorphous phase through a single melting transition at a temperature

equal to or higher than T_2. However, the observed DSC curve of the annealed HDPE in Fig. 3b shows two distinct melting transitions, which is different from a single peak expected from the melting-recrystallization model. Furthermore, we performed another DSC measurement with different heating rates because the kinetic nature of the simultaneous occurrence of melting and crystallization can be affected by heating rate.[4, 5] Figure S4 shows the DSC results acquired with 50 and 100 times faster heating rates than those in Fig. 3. Both DSC curves from the pristine and annealed HDPE samples show two melting peaks. The absence of a scanning rate effect on the number of melting peaks indicates that recrystallization via melt-crystallization is less likely to be responsible for the observed multiple melting peaks.

On the other hand, both the pre-melting via mesophases model and the melting of multi-thickness lamellae model can explain the observed annealing effect. In the mesophase, the annealing process would make the orthorhombic lamellae thicker. Subsequently, the thicker lamellae would result in higher temperatures for both the orthorhombic-to-mesophase and the mesophase-to-amorphous transitions,[44] as was reported for phase transitions in *n*-alkanes.[36] In the melting of multi-thickness lamellae model, the annealing could thicken both thinner and thicker lamellae, which would result in shift in melting temperatures. The presented DSC study with a controlled heat treatment is helpful for characterization of the PE melting phenomenon to a certain degree but is still not sufficient to lead to a conclusion on the underlying origin of the multiple melting transitions.

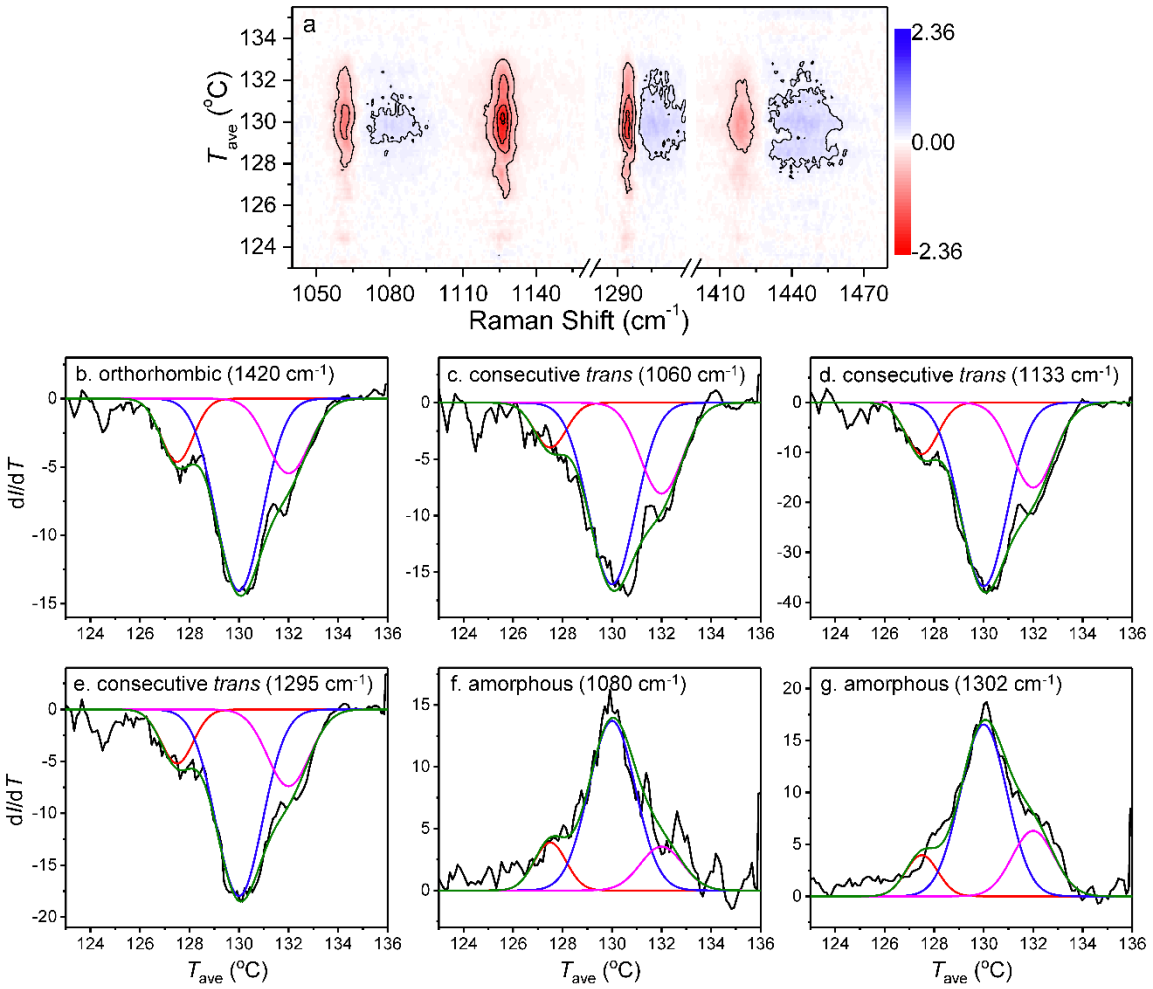

Figure 5. Least squares moving-window (LSMW) analysis of the HDPE Raman spectra from Sample I with the window size of eleven spectra (ΔT = 1 °C). (a) A contour map of the first order derivative (dI/dT) as a function of T_{ave} of a moving window. The dI/dT of six Raman peaks are plotted after numerically integrated over frequency ranges to cover the Raman peaks: (b) 1415 cm^{-1} to 1425 cm^{-1}, (c) 1056 cm^{-1} to 1068 cm^{-1}, (d) 1115 cm^{-1} to 1136 cm^{-1}, (e) 1290 cm^{-1} to 1299 cm^{-1}, (f) 1069 cm^{-1} to 1102 cm^{-1} and (g) 1299 cm^{-1} to 1325 cm^{-1}. The dI/dT plots are fitted with three Gaussian functions with respect to T_{ave}, and the details are found in the text.

Variable temperature Raman spectroscopy provides much richer information on specific conformations or structures of PE.[41] However, as shown in Fig. S2, the poor signal-to-noise ratio from the conventional single-step differential analysis based on individual peak intensity cannot allows for quantitative analysis of the multiple melting transitions. We use the LSMW method, an extended type of Savitzky–Golay differentiation, to calculate the first order derivative with respect to temperature.[38] Figure 5a shows the contour map of the first order derivative (dI/dT) as a function of the average temperature (T_{ave}) of a moving window. The window size of ΔT = 1 °C, which corresponds to eleven temperature steps, is used for a maximum signal-to-noise ratio without compromising the resolving power for this data set of HDPE Raman spectra. The positive (blue) and negative (red) contours show that conformational change occurs over a wide temperature range from 126 °C to 134 °C. For a quantitative analysis of conformation specific Raman modes, we separately plot dI/dT as a function of T_{ave} for the six representative Raman bands, as shown in Fig. 5b–5g. The negative sign of dI/dT in Fig. 5b–5e indicates that the Raman peak intensities corresponding to the orthorhombic and consecutive *trans* conformations decrease as temperature increases. The positive sign of dI/dT in Fig. 5f and 5g indicates that the Raman peak intensities corresponding to the amorphous conformation increase as temperature increases. It is noted that the overall shape of the dI/dT curves are similar. More importantly, all the dI/dT curves exhibit multiple transitions, which is similar in peak shape and relative peak position to the DSC curve in Fig. 3a. We fit the dI/dT curves with three Gaussian functions to determine the peak temperature, the full-width-half-maximum (FWHM), and the area of each underlying melting peak. First, the dI/dT curves of the orthorhombic and consecutive *trans* bands in Fig. 5b–5e are fitted with three peaks by

sharing their peak temperatures and FWHMs but setting their amplitudes free. Then, for the amorphous bands in Figs. 5f and 5g, we used the peak temperatures and FWHMs calculated from the fitting results of Fig. 5b–5e to avoid unwanted error propagation from the poor signal-to-noise ratio of the amorphous data. Figures 5b–5g show that the three Gaussian functions fit all the curves reasonably well even with a constraint of the shared peak temperatures and FWHMs. The determined peak temperatures of the three transition modes are 127.5 °C, 130.0 °C and 132.0 °C, and the determined FWHMs are 1.5 °C, 2.2 °C and 2.0 °C, respectively. The difference in melting peak locations between the DSC in Fig. 3 and the Raman LSMW results in Figure 5 can be due to difference in measurement volume and possible inaccuracy in temperature reading of the Raman sample stage. However, the overall shape (in relative peak positions and peak heights) of the melting trend is similar between DSC measurements and the LSMW analysis of the Raman spectra.

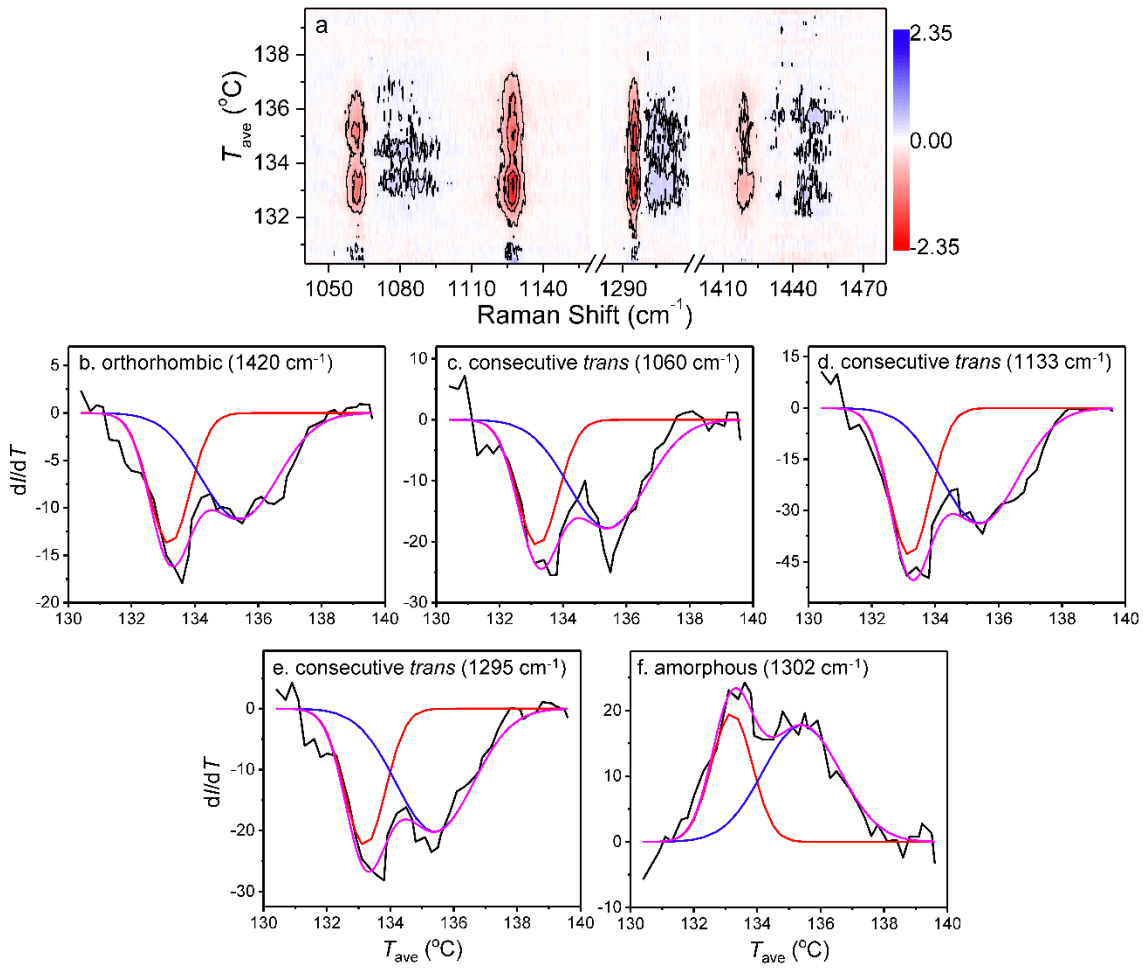

Figure 6. LSMW analysis of the HDPE Raman spectra from Sample II with the window size of five spectra (ΔT = 1 °C). (a) A contour map of dI/dT as a function of T_{ave} of a moving window. The dI/dT of five Raman peaks are plotted after numerically integrated over the same frequency ranges as Fig. 5. The dI/dT plots are fitted with two Gaussian functions with respect to T_{ave}.

Table 1. Ratios of the peak area of the underlying melting peaks to the peak area of the highest melting peak. The peak areas are determined from the LSMW results acquired from

the two HDPE samples in Figs. 5 and 6. For example, $A_{127.5}/A_{130.0}$ indicates the ratio of the area of the underlying peak centered at 127.5 °C to that of the peak centered at 130.0 °C.

Vibration mode		Sample I		Sample II
Frequency/ cm^{-1}	Assignment	$A_{127.5}/A_{130.0}$	$A_{132.0}/A_{130.0}$	$A_{133.2}/A_{135.4}$
1060	Consecutive *trans*	0.17 ± 0.05[a]	0.45 ± 0.07	0.61 ± 0.14
1133	Consecutive *trans*	0.19 ± 0.02	0.42 ± 0.06	0.67 ± 0.11
1295	Consecutive *trans*	0.20 ± 0.03	0.37 ± 0.05	0.58 ± 0.09
1420	Orthorhombic	0.23 ± 0.02	0.35 ± 0.05	0.65 ± 0.12
1080	Amorphous	0.19 ± 0.04	0.23 ± 0.20	N/A
1302	Amorphous	0.17 ± 0.03	0.35 ± 0.20	0.58 ± 0.09

[a]The uncertainty is calculated with the error propagation model for division by using the relative standard deviation of the fitting residuals within the FWHM range of each peak.

For a quantitative analysis, we calculate the area ratio of each side peak to the center peak (the highest amplitude) for each Raman band. The results of the six Raman bands are listed in Table 1. The area ratio for different conformation-specific Raman bands can provide direct information on conformational changes associated with each melting transition. Interestingly, the area ratios of the underlying peaks are similar among the different conformations, which indicates that conformational changes occur in the same way at each underlying transition temperature. This conformational similarity between multiple transitions are quite different from the behavior of *n*-alkane (n-$C_{21}H_{44}$). In Fig. S3, the orthorhombic peak of n-$C_{21}H_{44}$ shows a greater intensity variation at the lower phase transition temperature (orthorhombic-to-rotator) while the consecutive *trans* peaks and the

amorphous peaks show greater variations at the higher phase transition temperature (rotator-to-amorphous).

To confirm that this observation can be generalized for HDPE, we acquired another series of variable temperature Raman spectra from a differently prepared HDPE sample (called Sample II). Sample II was prepared from the same stock HDPE but crystallized during shear at a rate of 1 s^{-1} for 600 s. For Raman measurement, Sample II was heated at a different heating rate (0.25 °C/min) and temperature increment (0.25 °C). Figure 6 shows the LSMW results calculated from the Raman spectra of Sample II. Due to faster heating rate and wider temperature step, the first order derivative profiles look noisier than those from Sample I; however, both the contour maps and the temperature plots of individual Raman bands show at least two underlying melting peaks. The LSMW profiles were fitted reasonably well with two Gaussian functions when the peak temperature and the FWHM are shared. Similar to the results of Sample I, the relative areas for the five Raman bands (listed in Table 1) are similar among the Raman bands measured from Sample II, which reconfirms qualitative similarity in conformational changes at each underlying transition temperature. Interestingly, the values of the relative area acquired from Sample II are different from those from Sample I, indicating that thermal history of a sample can affect the relative amount of conformational change associated with the melting peak area and possibly the number of melting peaks.

The similarity in conformational changes at all underlying melting peaks provides insight into the remaining two models for the dominant origin of multiple melting peaks. First, in the pre-melting via mesophases model, the phase transitions at the lower temperatures in

Fig. 5 could be considered to correspond to orthorhombic-to-mesophase$_a$ and mesophase$_a$-to-mesophase$_b$ transitions, and the transition at the highest temperature would be mesophase$_b$-to-amorphous transition. In this case, conformational changes across all transitions must be different because the initial (orthorhombic) conformation and the final (amorphous) conformation are different. For example, in *n*-alkanes, the orthorhombic-to-rotator and the rotator-to-amorphous transitions appear differently in the orthorhombic, consecutive *trans*, and amorphous Raman bands. Therefore, the pre-pelting via mesophases model is not consistent with the conformational similarity of all underlying melting peaks observed from the LSMW Raman results. The negligible mesophase contribution is consistent with the Raman study of a series of *n*-alkane by Kotula et al.[36] They reported that the contribution of rotator phases become negligible in mass fraction when the chain length n > 40. PE can be considered as an extrapolated case of a long chain alkane that has only direct transition from the crystalline phase to the amorphous phase.

Next, the melting of multi-thickness lamellae model assumes that all underlying melting transitions are qualitatively the same in terms of conformational change, which is consistent with the observed conformational similarity of all underlying melting peaks. In the melting of multi-thickness lamellae model, the underlying peak area will be proportional to the crystallinity change due to melting of the corresponding lamella. In other words, the overall LSMW Raman profiles can be considered as the mass weighted thickness distribution function of PE lamellae. The thermal history of a HDPE sample can affect not only the number of melting peaks but also their widths, as demonstrated by the annealing effect in Fig. 3b and Fig. S4b. The multiple melting peaks observed from Sample I in DSC measurements clearly demonstrate the heterogeneity in HDPE melting, and the

conformational similarity in the multiple melting peaks revealed by Raman LSMW analysis suggests a broad multimodal distribution of lamella thickness as the main reason for the observed heterogeneity.

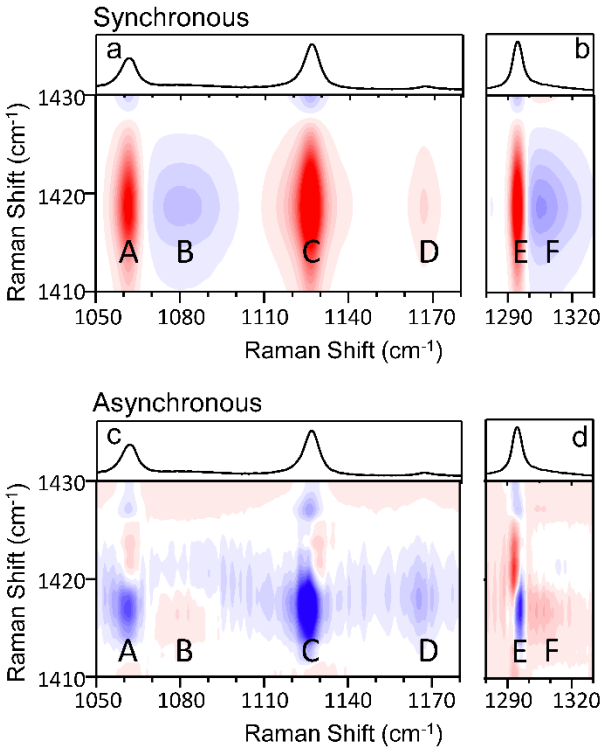

Figure 7. Two-dimensional correlation spectroscopy (2DCOS) analysis of the temperature dependent Raman spectra of the HDPE Sample I over the temperature range from 121.2 °C to 136.3 °C. The red and blue colors denote positive and negative cross peaks, respectively.

Now, we discuss the contribution of non-crystalline *trans*-rich conformations to the observed HDPE melting. We used the two-dimensional correlation spectroscopy (2DCOS) method, which has been widely used to find the pair-wise correlation of spectral changes with respect to external perturbation (e.g., temperature).[45] Briefly, 2DCOS calculates the

complex cross correlation of spectral intensity variations in response to an external perturbation for each frequency pair. The real (in-phase) term of the cross correlation is used to construct the synchronous map, and the imaginary (out-of-phase) term is used to construct the asynchronous map. The signs of the synchronous and asynchronous maps indicate the direction and the sequence, respectively, of the intensity changes for the corresponding frequency pair. Figure 7 shows the synchronous and asynchronous 2DCOS maps calculated from the variable-temperature Raman spectra, which was used for Figs. 1 and 5. The synchronous map in Fig. 7a shows correlations between the orthorhombic peak and other six peaks corresponding to the consecutive *trans* and amorphous conformations. The synchronous correlation reconfirms positive and negative correlation between the orthorhombic peak and the consecutive *trans* peaks and between the orthorhombic peak and the amorphous peaks, respectively. It is interesting that the asynchronous map in Fig. 7b shows non-zero features, indicating that there is out-of-phase intensity change between peaks. According to Noda's rule,[45] the combination of the positive sign in the synchronous map and the negative sign in the asynchronous map indicates that the orthorhombic peak (1419 cm^{-1}) decreases earlier than the consecutive *trans* peaks (1062 cm^{-1}, 1127 cm^{-1}, 1168 cm^{-1} and 1295 cm^{-1}) decrease. Similarly, the negative sign in the synchronous map and the positive sign in the asynchronous map indicates that the orthorhombic peak (1419 cm^{-1}) decreases earlier than the amorphous peaks (1080 cm^{-1} and 1302 cm^{-1}) increase. The out-of-phase spectral changes suggest that there exists the NCCT conformation between the orthorhombic and the amorphous phases. The evidence of a third phase, represented by the NCCT bands in the Raman spectrum, has been questioned for PE due to the large uncertainty in the relative amount of this phase in highly crystalline samples and the

variation in fitting routines for the multiple overlapped Raman peaks.[46] Although assessment of a third phase is challenging at lower temperatures, Migler *et al*. have observed the presence of NCCT bands in the Raman spectrum prior to the appearance of crystallinity during isothermal crystallization.[35] Raman measurements on the melting of alkanes have helped to further explain the NCCT bands as not necessarily arising due to a separate *phase*, but from the fraction of chain segments not in an orthorhombic packing that have approximately 4 or more consecutive *trans* bonds prior to the appearance of a *gauche* bond.[36]

For quantitative information of the NCCT contribution, we calculate the mass fractions of the orthorhombic and the consecutive *trans* conformations from the Raman peak intensities of Fig. 1b by using the method in Ref. 35. The mass fraction of the NCCT is calculated by the subtraction of the orthorhombic mass fraction from the consecutive *trans* mass fraction. We assume a negligible NCCT mass fraction before melting and scale the consecutive *trans* curve at 121 °C to the crystallinity (56.1 ± 0.1)% measured by the DSC curve in Fig. 3a. Interestingly the mass fraction of the mesophase departs from zero at 127 °C, reaches about 10% at the maximum at 130 °C and then returns to zero at 133 °C. Note that in the temperature window from roughly 132.5 °C to 133 °C, there is no detectable crystallinity but there is a small contribution from the NCCT conformations. This small fractional contribution is consistent with the previous report on a Raman analysis of an early stage crystallization of isothermally cooled HDPE.[35] Despite the poor signal-to-noise ratio, the non-zero region of the NCCT curve in Fig. 8 seems to match the three underlying peaks of the dI/dT curves in Fig. 5, which indicates that this conformational state does not contribute exclusively to one melting peak.

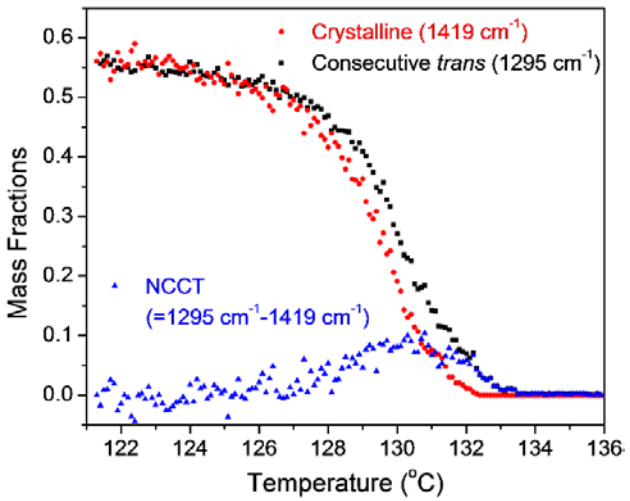

Figure 8. Mass fractions of the crystalline, consecutive *trans*, non-crystalline consecutive *trans* (NCCT) conformations estimated from the Raman spectra of Sample I in Fig. 1. The mass fraction of the crystalline conformation is calculated by scaling the plot for the orthorhombic peak at 1419 cm^{-1} (in Fig. 1b) to the crystallinity determined from the DSC measurement in Fig. 3a. Similarly, the mass fraction of the consecutive *trans* conformation is calculated by scaling the plot for the peak at 1295 cm^{-1} (in Fig. 1b) to the crystallinity value, based on assumption that consecutive *trans* conformation exists in the crystalline phase at a sufficiently lower temperature than the melting transitions. The mass fraction of the NCCT conformation is calculated by subtracting the mass fraction of the orthorhombic crystalline conformation from the mass fraction of the consecutive *trans* conformation.

The NCCT fraction can be put into the context of prior NMR experiments on PE, which are sensitive to chain motion consisting of a 180° rotation and a translation of one repeat unit within the orthorhombic packing. The frequency of these events can approach 10^5 s^{-1} near the melting temperature,[47] and additional NMR measurements have revealed a second, slower translation-rotation motion that occurs in more perfect crystallites.[48] For

comparison, the vibrational modes accessed with Raman spectroscopy are of order 10^{13} vibrations per second,[34] so we can consider the vibrational modes effectively decoupled from the chain translation-rotation events resolved in NMR. We must also consider the time-average fraction of chains that are undergoing this chain diffusion at a given instant. Milner and Wentzel have concluded from free energy arguments that the concentration of these events must be very dilute in the orthorhombic crystal: given the formation energy E = 100 kJ/mol from NMR measurements, the concentration is expected to be of order $e^{-E/kT} \sim 10^{-13}$ per chain.[49] Simulations indicate a much lower formation energy (of order kT) in some rotator phases of alkanes, meaning that the concentration of these events would also be significantly increased.[49] However, our LSMW analysis does not reveal a strong phase transition during melting.

A combination of multiple spectral analysis methods (principal component analysis, peak fitting, LSMW, and 2DCOS) and a thermal analysis method (DSC with and without annealing) can therefore be used to characterize the complex changes in conformation and thermodynamics during HDPE melting. Those multidimensional analysis results allow one to understand not only the dominant mechanism but also minor mechanisms that contribute to the observed heterogeneous melting. These techniques could be combined with in-situ X-ray scattering methods to simplify the complications associated with analyzing scattering data to further understand the structural and conformational changes during melting at different length scales.[20]

CONCLUSION

We have investigated the conformational evolution during the melting of HDPE samples with complex thermal pretreatment by variable temperature Raman spectroscopy and DSC. We have identified the dominant origin of the multiple melting peaks by analyzing the noise-suppressed first order derivative of Raman intensity with respect to temperature calculated with the LSMW method. We examined three different models that could be used to explain the multiple melting peaks observed by DSC: the melting-recrystallization model, the pre-melting via mesophases model, and the melting of multi-thickness lamellae model. The dominant melting mechanism has been evaluated by the annealing effect on the DSC results and the LSMW analysis of Raman spectra. The similarity in conformational change across all underlying melting peaks strongly suggests direct transition from the crystalline phase to the amorphous phase, without going through a measurable amount of mesophase or recrystallization intermediates. These results strongly suggest that for the thermal pretreatments examined that the dominant mechanism of the heterogeneous melting transition is consistent with the melting of multi-thickness lamellae model. However, the two-dimensional correlation analysis followed by mass fraction estimation from the Raman spectra implies that the non-crystalline consecutive *trans* conformations may exist by less than 10% in mass fraction during melting.

AUTHOR INFORMATION

Corresponding Author

*E-mail: youngjong.lee@nist.gov

Author Contributions

Y.J. and A.P.K. contributed equally.

Notes

The authors declare no competing financial interest.

ACKNOWLEDGMENT

Ying Jin acknowledges the support from the NIST Biomanufacturing Program.

DISCLAIMER

Certain commercial equipment, instruments, or materials are identified in this paper in order to adequately specify the experimental procedure. Such identification does not imply recommendation or endorsement by the National Institute of Standards and Technology, nor does it imply that the materials or equipment identified are necessarily the best available for the purpose.

REFERENCES

(1) Cheng, S. Z. D., *Phase transitions in polymers: the role of metastable states*. Elsevier: **2008**.
(2) Tashiro, K.; Sasaki, S. and Kobayashi, M. Structural investigation of orthorhombic-to-hexagonal phase transition in polyethylene crystal: The experimental confirmation of the conformationally disordered structure by X-ray diffraction and infrared/Raman spectroscopic measurements. *Macromolecules* **1996**, 29(23), 7460-7469.
(3) Muthukumar, M. Nucleation in Polymer Crystallization. *Adv Chem Phys* **2004**, 128, 1-63.
(4) Lippits, D. R.; Rastogi, S. and Hohne, G. W. H. Melting kinetics in polymers. *Phys Rev Lett* **2006**, 96(21), 218303.
(5) Pandey, A.; Toda, A. and Rastogi, S. Influence of Amorphous Component on Melting of Semicrystalline Polymers. *Macromolecules* **2011**, 44(20), 8042-8055.
(6) Wang, Y.; Chan, C. M.; Ng, K. M. and Li, L. What controls the lamellar orientation at the surface of polymer films during crystallization? *Macromolecules* **2008**, 41(7), 2548-2553.
(7) Hamad, F. G.; Colby, R. H. and Milner, S. T. Lifetime of Flow-Induced Precursors in Isotactic Polypropylene. *Macromolecules* **2015**, 48(19), 7286-7299.
(8) Fukushima, H.; Ogino, Y.; Matsuba, G.; Nishida, K. and Kanaya, T. Crystallization of polyethylene under shear flow as studied by time resolved depolarized light scattering. Effects of shear rate and shear strain. *Polymer* **2005**, 46(6), 1878-1885.
(9) Pople, J. A.; Mitchell, G. R.; Sutton, S. J.; Vaughan, A. S. and Chai, C. K. The development of organized structures in polyethylene crystallized from a sheared melt, analyzed by WAXS and TEM. *Polymer* **1999**, 40(10), 2769-2777.
(10) Tanabe, Y.; Strobl, G. R. and Fischer, E. W. Surface Melting in Melt-Crystallized Linear Polyethylene. *Polymer* **1986**, 27(8), 1147-1153.
(11) Suehiro, K.; Tanizaki, H. and Takayanagi, M. X-Ray Studies of Surface Melting in Single-Crystals of Linear Polyethylene. *Polymer* **1976**, 17(12), 1059-1062.
(12) Strobl, G. A thermodynamic multiphase scheme treating polymer crystallization and melting. *Eur Phys J E* **2005**, 18(3), 295-309.
(13) Cho, T. Y.; Stille, W. and Strobl, G. Zero growth temperature of crystallizing polyethylene. *Macromolecules* **2007**, 40(7), 2596-2599.
(14) Strobl, G. From the melt via mesomorphic and granular crystalline layers to lamellar crystallites: A major route followed in polymer crystallization? *Eur Phys J E* **2000**, 3(2), 165-183.
(15) Keller, A.; Hikosaka, M.; Rastogi, S.; Toda, A.; Barham, P. J. and Goldbeckwood, G. An Approach to the Formation and Growth of New Phases with Application to Polymer Crystallization - Effect of Finite-Size, Metastability, and Ostwald Rule of Stages. *J Mater Sci* **1994**, 29(10), 2579-2604.
(16) Marand, H. and Huang, Z. Y. Isothermal lamellar thickening in linear polyethylene: Correlation between the evolution of the degree of crystallinity and the melting temperature. *Macromolecules* **2004**, 37(17), 6492-6497.
(17) Rastogi, S.; Lippits, D. R.; Peters, G. W. M.; Graf, R.; Yao, Y. F. and Spiess, H. W. Heterogeneity in polymer melts from melting of polymer crystals. *Nat Mater* **2005**, 4(8), 635-641.

(18) Jarecki, L. and Misztal-Faraj, B. Kinetic model of polymer crystallization with the lamellar thickness distribution. *Eur Polym J* **2015**, 73, 175-190.
(19) Furushima, Y.; Nakada, M.; Murakami, M.; Yamane, T.; Toda, A. and Schick, C. Method for Calculation of the Lamellar Thickness Distribution of Not-Reorganized Linear Polyethylene Using Fast Scanning Calorimetry in Heating. *Macromolecules* **2015**, 48(24), 8831-8837.
(20) Crist, B. SAXS studies of polymer melting: Models for surface melting, sequential melting, and stack melting. *Macromolecules* **2003**, 36(13), 4880-4890.
(21) Rastogi, S.; Spoelstra, A. B.; Goossens, J. G. P. and Lemstra, P. J. Chain mobility in polymer system: on the borderline between solid and melt. 1. Lamellar doubling during annealing of polyethylene. *Macromolecules* **1997**, 30(25), 7880-7889.
(22) Vanaerle, N. A. J. M.; Lemstra, P. J. and Braam, A. W. M. A Real-Time X-Ray Melting Study of Partly Drawn Uhmw-Polyethylene. *Polym Commun* **1989**, 30(1), 7-10.
(23) Schultz, J. M.; Fischer, E. W.; Schaumburg, O. and Zachmann, H. A. Small-Angle X-Ray-Scattering Studies of Melting. *J Polym Sci B Polym Phys* **1980**, 18(2), 239-245.
(24) Toda, A.; Androsch, R. and Schick, C. Insights into polymer crystallization and melting from fast scanning chip calorimetry. *Polymer* **2016**, 91, 239-263.
(25) Matsuda, H.; Aoike, T.; Uehara, H.; Yamanobe, T. and Komoto, T. Overlapping of different rearrangement mechanisms upon annealing for solution-crystallized polyethylene. *Polymer* **2001**, 42(11), 5013-5021.
(26) Pak, J. and Wunderlich, B. Melting and crystallization of polyethylene of different molar mass by calorimetry. *Macromolecules* **2001**, 34(13), 4492-4503.
(27) Alamo, R. and Mandelkern, L. Origins of Endothermic Peaks in Differential Scanning Calorimetry. *J Polym Sci Pol Phys* **1986**, 24(9), 2087-2105.
(28) Watanabe, S.; Dybal, J.; Tashiro, K. and Ozaki, Y. A near-infrared study of thermally induced structural changes in polyethylene crystal. *Polymer* **2006**, 47(6), 2010-2017.
(29) Mizushima, M.; Kawamura, T.; Takahashi, K. and Nitta, K. In situ near-infrared spectroscopic studies of the structural changes of polyethylene during melting. *Polym J* **2012**, 44(2), 162-166.
(30) Kurelec, L.; Rastogi, S.; Meier, R. J. and Lemstra, P. J. Chain mobility in polymer systems: On the borderline between solid and melt. 3. Phase transformations in nascent ultrahigh molecular weight polyethylene reactor powder at elevated pressure as revealed by in situ Raman spectroscopy. *Macromolecules* **2000**, 33(15), 5593-5601.
(31) Strobl, G. R. and Hagedorn, W. Raman-Spectroscopic Method for Determining Crystallinity of Polyethylene. *J Polym Sci B Polym Phys* **1978**, 16(7), 1181-1193.
(32) Weeks, J. J. Melting Temperature and Change of Lamellar Thickness with Time for Bulk Polyethylene. *J Res NBS A Phys Chem* **1963**, 67A(5), 441-451.
(33) Uehara, H.; Yamanobe, T. and Komoto, T. Relationship between solid-state molecular motion and morphology for ultrahigh molecular weight polyethylene crystallized under different conditions. *Macromolecules* **2000**, 33(13), 4861-4870.
(34) Koenig, J. L., *Infrared and Raman Spectroscopy of Polymers*. Rapra Technology Ltd.: **2001**.
(35) Migler, K. B.; Kotula, A. P. and Hight Walker, A. R. Trans-Rich Structures in Early Stage Crystallization of Polyethylene. *Macromolecules* **2015**, 48(13), 4555-4561.

(36) Kotula, A. P.; Hight Walker, A. R. and Migler, K. B. Raman analysis of bond conformations in the rotator state and premelting of normal alkanes. *Soft Matter* **2016**, 12(22), 5002-5010.
(37) Lee, Y. J. Analytical and Numerical Characterization of Autocorrelation and Perturbation-Correlation Moving-Window Methods. *Appl Spectrosc* **2017**, 71(6), 1321-1333.
(38) Lee, Y. J. Least-Squares Moving-Window Spectral Analysis. *Appl Spectrosc* **2017**, published online; DOI: 10.1177/0003702816685336.
(39) Hoeve, C. A. J.; Wagner, H. L. and Verdier, P. H. Characterization of Linear Polyethylene SRM 1475 .1. Introduction. *J Res NBS A Phys Chem* **1972**, 76A(2), 137-140.
(40) Kotula, A. P.; Meyer, M. W.; De Vito, F.; Plog, J.; Hight Walker, A. R. and Migler, K. B. The rheo-Raman microscope: Simultaneous chemical, conformational, mechanical, and microstructural measures of soft materials. *Rev Sci Instrum* **2016**, 87(10), 105105.
(41) Jin, Y.; Kotula, A. P.; Hight Walker, A. R.; Migler, K. B. and Lee, Y. J. Phase-specific Raman analysis of *n*-alkane melting by moving-window two-dimensional correlation spectroscopy. *J Raman Spectrosc* **2016**, 47(11), 1375-1384.
(42) Zhang, X. B.; Li, Z. S.; Lu, Z. Y. and Sun, C. C. The reorganization of the lamellar structure of a single polyethylene chain during heating: Molecular dynamics simulation. *J Chem Phys* **2001**, 115(21), 10001-10006.
(43) Muller, A. J.; Arnal, M. L. Thermal fractionation of polymers. *Prog Poly Sci* **2005**, 30(5), 559-603.
(44) Rastogi, S.; Kurelec, L. and Lemstra, P. J. Chain mobility in polymer systems: On the borderline between solid and melt. 2. Crystal size influence in phase transition and sintering of ultrahigh molecular weight polyethylene via the mobile hexagonal phase. *Macromolecules* **1998**, 31(15), 5022-5031.
(45) Noda, I. Generalized 2-Dimensional Correlation Method Applicable to Infrared, Raman, and Other Types of Spectroscopy. *Appl Spectrosc* **1993**, 47(9), 1329-1336.
(46) Naylor, C. C.; Meier, R. J.; Kip, B. J.; Williams, K. P. J.; Mason, S. M.; Conroy, N. and Gerrard, D. L. Raman Spectroscopy Employed for the Determination of the Intermediate Phase in Polyethylene. *Macromolecules* **1995**, 28(8), 2969-2978.
(47) Schmidt-Rohr, K. and Spiess, H. W. Chain diffusion between crystalline and amorphous regions in polyethylene detected by 2D exchange carbon-13 NMR. *Macromolecules* **1991**, 24(19), 5288-5293.
(48) Hillebrand, L.; Schmidt, A.; Bolz, A.; Hess, M.; Veeman, W.; Meier, R. J. and van der Velden, G. Nuclear Magnetic Resonance Detection of Two Distinctly Different Chains in the Orthorhombic Crystalline Phase of Polyethylenes. *Macromolecules* **1998**, 31(15), 5010-5021.
(49) Wentzel, N. and Milner, S. T. Simulation of multiple ordered phases in C_{23} *n*-alkane. *J Chem Phys* **2011**, 134(22), 224504.

Table of contents